Cross-species cortical alignment identifies different types of neuroanatomical reorganization in higher primates

Nicole Eichert[1,*], Emma C. Robinson[2], Katherine L. Bryant[3], Saad Jbabdi[1], Mark Jenkinson[1], Longchuan Li[4], Kristine Krug[5], Kate E. Watkins[6] & Rogier B. Mars[1,3]

[1] Wellcome Centre for Integrative Neuroimaging, Centre for Functional MRI of the Brain (FMRIB), Nuffield Department of Clinical Neurosciences, John Radcliffe Hospital, University of Oxford, Oxford, OX3 9DU, United Kingdom
[2] Biomedical Engineering Department, King's College London, London, WC2R 2LS, United Kingdom
[3] Donders Institute for Brain, Cognition and Behaviour, Radboud University Nijmegen, 6525 HR Nijmegen, The Netherlands
[4] Marcus Autism Center, Children's Healthcare of Atlanta, Emory University, Atlanta, GA 30329, United States of America
[5] Department of Physiology, Anatomy and Genetics, University of Oxford, Oxford, OX1 3PT, United Kingdom
[6] Wellcome Centre for Integrative Neuroimaging, Department of Experimental Psychology, University of Oxford, Oxford, OX2 6GG, United Kingdom

* Correspondence:
Nicole Eichert
Wellcome Centre for Integrative Neuroimaging
Nuffield Department of Clinical Neurosciences
John Radcliffe Hospital
University of Oxford
Oxford OX3 9DU
United Kingdom
E-mail: nicole.eichert@psy.ox.ac.uk

Abstract

Evolutionary adaptations can affect different aspects of brain architecture, including areal expansion, relocation, or changes in connectivity profiles. Distinguishing between different types of reorganization is critical for our understanding of brain evolution. We propose to address this using a computational neuroanatomy approach. We investigate the extent to which between-species cortical alignment based on myelin can predict changes in connectivity patterns across macaque, chimpanzee and human brains. We show that expansion and relocation of brain areas as predicted by the myelin-based alignment are sufficient to predict reorganization of several white matter tracts and their terminations in temporal, frontal and parietal cortex. A notable exception is the arcuate fasciculus, in which we found extensive tract extension into new territories that cannot be explained by cortical expansion. The presented approach can flexibly be extended to include other features of cortical organization and other species, which allows us to directly test and quantify evolutionary hypotheses.

Introduction

Comparative neuroscience aims foremost to identify how each species' brain adapted to its owner's ecological niche. But the great challenge of the field is to generalize these insights to define a unifying theory of brain evolution that can account for both shared features across brains and specializations of particular lineages or species (Krubitzer, 2009).

Differences in brain organization can come in many forms (Krubitzer and Kaas, 2005; Mars et al., 2017; Rogier B. Mars et al., 2018a) and dissociating them is challenging (Figure1A, B). For instance, given an ancestral or reference state, local expansions of the cortical sheet can lead to the relocation of homologous areas between two species. As a case in point, human MT+ complex is located much more ventrally in posterior temporal cortex than its macaque homolog (Huk et al., 2002). Such cortical relocations also affect the location of connections of these areas, but this situation is distinct from the scenario in which a tract extends into new cortical territory. These two scenarios are illustrated in Figure 1B. The top red area has expanded, leading to a relocation of the blue area with respect to the purple and yellow area. The connections of the areas do not change in this scenario, resulting in a relocation of the connections of the blue area. In the bottom figure, a tract's terminations have invaded a neighboring territory, but this change is independent from cortical expansion. Thus, in both cases the connections are located in a different location from those in the ancestral state, but the causes are different.

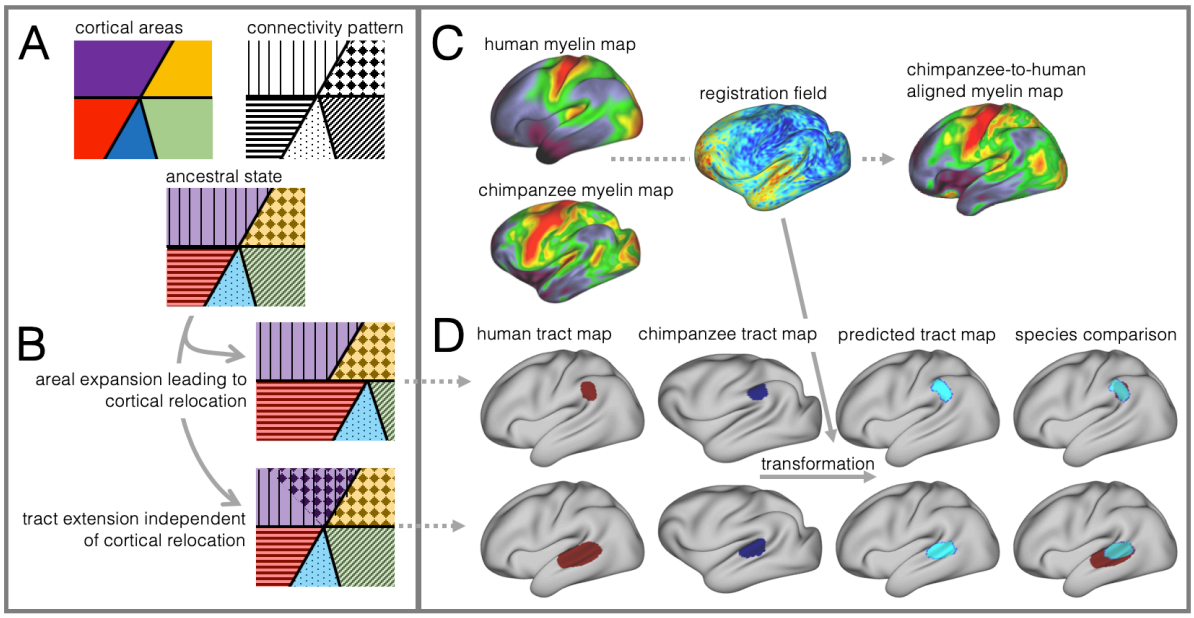

Figure 1. Cortical specializations. **A**: The cortical organization can be described using different modalities such as brain areas defined by myelin content (top left) or the pattern of brain connections (top right). **B**: Anatomical changes can affect both modalities differentially. Top and bottom panel show different evolutionary scenarios. **C**: Alignment of homologous brain areas derived from myelin maps can model cortical expansion across species, here shown for human and chimpanzee. **D**: Applying the cross-species registration field to surface tract maps allows us to distinguish evolutionary scenarios. Here shown are toy example maps of one tract that changed due to areal expansion and relocation alone (top panel) and one tract that additionally extended into new brain areas (bottom panel).

Traditionally, different evolutionary scenarios are difficult to distinguish, as this requires data from multiple modalities and from many cortical areas in the species under study. The need for cartography of a large range of species to infer evolutionary principles is well acknowledged (Striedter et al., 2014), but inferring principles of evolutionary change in brain organization also requires methods to formally compare brains of multiple species.

We propose a framework that allows one to test among different forms of cortical reorganization by registering brains together into a single shared coordinate system (Figure 1C,D). Such an approach allows us to place the different brains into a common space based on one feature and then compare the results to registration based on another feature. This 'common space' concept proved feasible in a previous study testing whether the extension of the human arcuate fasciculus (AF) compared with the macaque AF could be accounted for by differential cortical expansion between the two brains (Eichert et al., 2019a). In the present study, we generalize this approach to develop a cross-species registration based on a multimodal surface matching (MSM) algorithm (Robinson et al., 2018, 2014, 2013) to derive a cortical registration between different species.

We based our registration framework on whole brain neuroimaging data of macaque, chimpanzee and human brains. Neuroimaging allows one to acquire high-resolution data from the same brains using different modalities within a short time. The digital nature of the data allows easy manipulation, making it ideal for the present purposes (Thiebaut de Schotten et al., 2019). As primary modality we use surface maps derived from the cortical ribbon of T1- and T2-weighted scans, which have been shown to correlate well with cortical myelinization and which are available and all three species (Glasser and Van Essen, 2011). Such 'myelin maps' can be used to identify homologous areas across brains and species, such as primary sensory and motor cortex, which is high in myelin, and association cortex which is low in myelin (Glasser et al., 2014; Large et al., 2016). As second modality, we use diffusion MRI tractography to reconstruct long range white matter fibers of the cortex to establish its connections (Hecht et al., 2015; Rogier B Mars et al., 2018b).

Given data from these two modalities, we developed an approach to reveal different types of cortical reorganization. First, we register the cortical surfaces of the different species to one another based on myelin maps (Figure 1C). This cortical alignment uses the distinction of primary and higher order areas in myelin maps as anchor points across all three species. Next, we apply this registration to overlay homologous parts of the cortex and to calculate the underlying distortions of the cortical sheet. This registration field effectively models areal expansion or contraction underlying cortical relocation of homologous areas. We then apply this registration to the cortical projection maps of white matter tracts to assess how well the myelin-based registration can predict changes in tract projection patterns across species (Figure 1D). A good prediction, i.e. a high overlap of the tract maps, indicates that cortical expansion and relocation of targets zones alone can predict tact projections (Figure 1D, top), a poor prediction indicates that the tract is reaching new cortical territory (Figure 1D, bottom).

Here, we aim to distinguish different scenarios of cortical evolution for a set of major cortical white matter tracts. We focus our analysis in particular on tracts terminating in posterior temporal, inferior parietal, and occipital cortex, which have well described myelin markers and cortical connections (Glasser et al., 2014; Large et al., 2016; Mars et al., 2013; Ruschel et al., 2014). We selected tracts whose homology across species has been shown, but which are also thought to have undergone substantial reorganization among different primate species (Mars et al., 2013; Roumazeilles et al., n.d.; Van Essen and Dierker, 2007). In the case of the human arcuate fasciculus (AF), for example, it has been suggested that the tract's projections extended into new areas in the middle temporal lobe (Rilling et al., 2008). For other tracts, such as the inferior fronto-occipital fasciculus (IFO), however, the tract terminations have been found to be similar across primates when they were assessed in terms of their areal projections (Mars et al., 2016). For the superior longitudinal fasciculus (SLF3), an evolutionary trajectory has been described for the frontal extensions that suggests that SLF3 reaches more anterior territory in the human (Bryant and Mars, 2019; Hecht et al., 2013). All such proposed adaptations in brain organization, however, need to be assessed in relation to other types of reorganization. By applying a cross-species registration we can infer if only cortical relocation was affecting a tract's connectivity profile or if a tract is reaching into new cortical territory.

Results

We set out to investigate different types of cortical reorganization between macaque, chimpanzee, and human brains. First, we investigated cortical relocation of brain areas by registering myelin maps of the cortical surface to one another and derived the local distortions required. Second, we used the resulting mesh deformations to transform maps of cortical projections of major white matter tracts. This allowed us to assess how well the myelin registration predicts actual projection maps across species, providing an index of tract extensions in the human brain.

Myelin Registration

We developed a surface registration between species based on myelin maps using MSM. Figure 2 shows the final results of chimpanzee to human, macaque to chimpanzee, and macaque to human brain registrations. The cross-species registration aligns the myelin maps well, with the predicted human maps showing most of the distinctive features of the actual human myelin map (Figure 2, top row). Posterior areas such as V1 are well aligned, with the highest myelin evident on the medial part of the occipital cortex, having relocated quite substantially from a more lateral orientation in the macaque. The prominent myelin hot spot in the location of the MT+ complex is also noticeable. Areas where the myelin maps showed fewer distinctive features to guide the registration, such as in the prefrontal cortex, showed some differentiation between the predicted and actual human maps. Correlation maps of the human myelin maps and the predicted myelin maps as well as the deformation fields underlying the registrations are provided in the Supplementary Material (Figure S2).

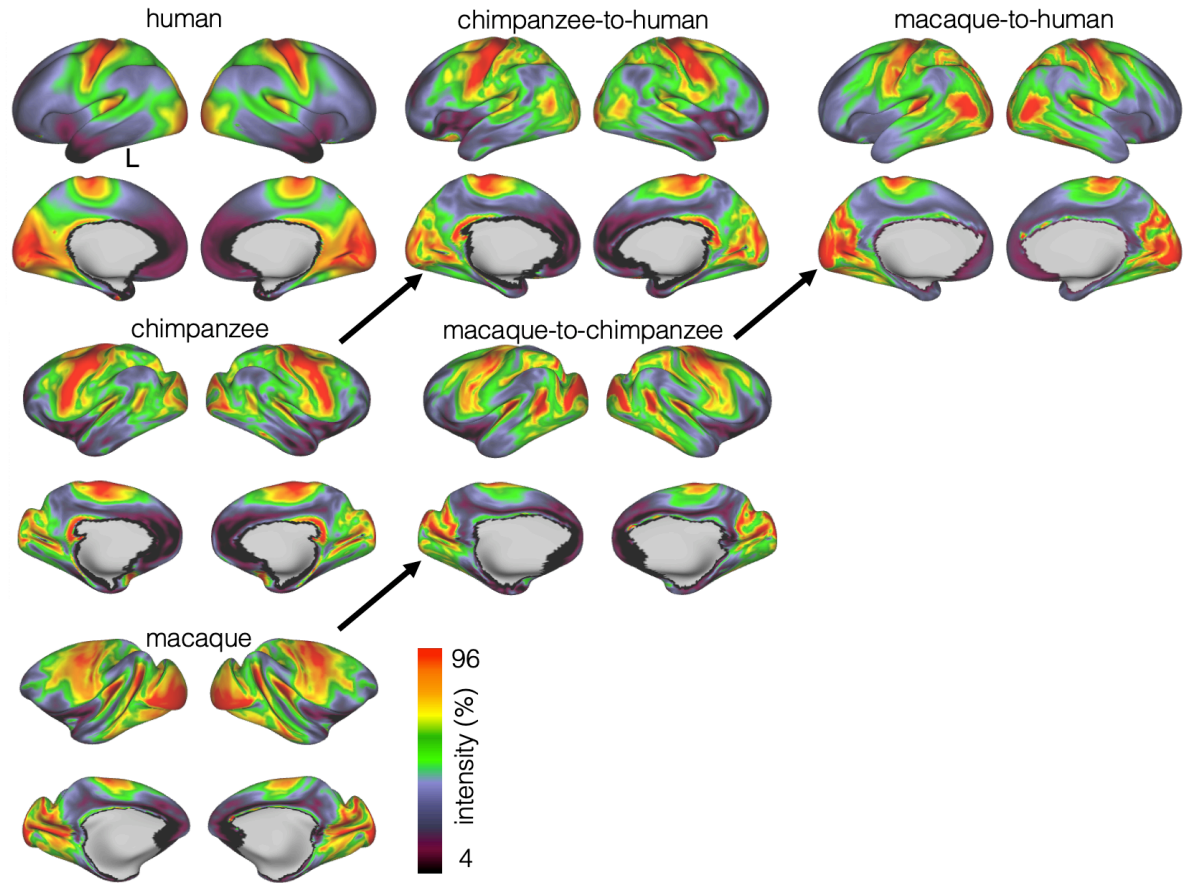

Figure 2. Myelin registration. Species average myelin maps of the three species (left panel) and myelin maps resampled across species after applying the MSM-derived registration.

Tract Maps

We constructed the cortical projection maps of the following tracts in all three species: Cortico-spinal tract (CST), middle longitudinal fasciculus (MDLF), vertical occipital fasciculus (VOF) inferior fronto-occipital fasciculus (IFO), inferior longitudinal fasciculus (ILF), the third branch of the superior longitudinal fasciculus (SLF3), and the arcuate fasciculus (AF). We then applied the myelin-based surface registration to assess whether the cortical relocation demonstrated in the myelin registration above fully explains the changes in tracts. Figure 3 shows actual and predicted tract maps and for visual assessment a thresholded overlay of actual human and predicted tract maps is shown in Figure 4A.

We accessed the success of the myelin registration in predicting the tract projections in a number of ways. First, weighted correlation maps provide a visualization of the local quality of the prediction (Figure 4B,C). A high value means that the myelin registration alone is sufficient to predict a tract's projection in this part of the brain. A low correlation value indicates that reorganization of a tract's connectivity pattern took place in addition to cortical relocation modelled by the myelin registration. Second, the Dice coefficient of similarity provides a more general measure of similarity between the predicted and actual tract maps, where a Dice coefficient of '1' indicates perfect overlap and thus no tract extension into areas other than would be predicted by cortical relocation assessed using the myelin map

registration. Finally, we calculated a 'tract extension ratio' that indicates how much of the actual tract projections extend into parts of the surface not predicted, where a value of >1 indicates a tract extension into novel territory. Both the Dice coefficients and tract extension ratios were computed for thresholded tract maps defined by the human tract map covering 40% of the brain's surface, but the resulting pattern of values is robust across a range of thresholds (see Figure S3).

For the analyzed tracts, the actual cortical terminations that we derived match the connectivity patterns expected from the literature (Figure 3A,C,E). In general, it can be observed that the myelin-based registration can predict the tract maps well in both hemispheres, with the notable exception of AF and to a lesser extend ILF and SLF3 (Figure 3B,D). AF in particular shows the lowest Dice coefficient and the highest extension ratio (Figure 5). The maps for the macaque are overall less well predicted than for the chimpanzee, as can be seen in the overlay and correlation maps (Figure 4). This effect is captured in the Dice coefficients, which tend to be lower for the macaque (Figure 5B, Figure S3).

A statistical two-way analysis was performed in both hemispheres to assess the effect of species and tract on the extension ratios. In the left hemisphere, the analysis revealed a significant main effect of species ($F(1,99) = 10.26$, $p < 0.05$), tract ($F(6,99) = 845.64$, $p < 0.05$) and a significant interaction effect ($F(6,99) = 218.52$, $p < 0.05$). Similarly, in the right hemisphere, we found a significant main effect of species ($F(1,99) = 11.95$, $p < 0.05$), tract ($F(6,99) = 409.70$, $p < 0.05$) and a significant interaction effect ($F(6,99) = 285.91$, $p < 0.05$). We will discuss the various tracts in more detail below.

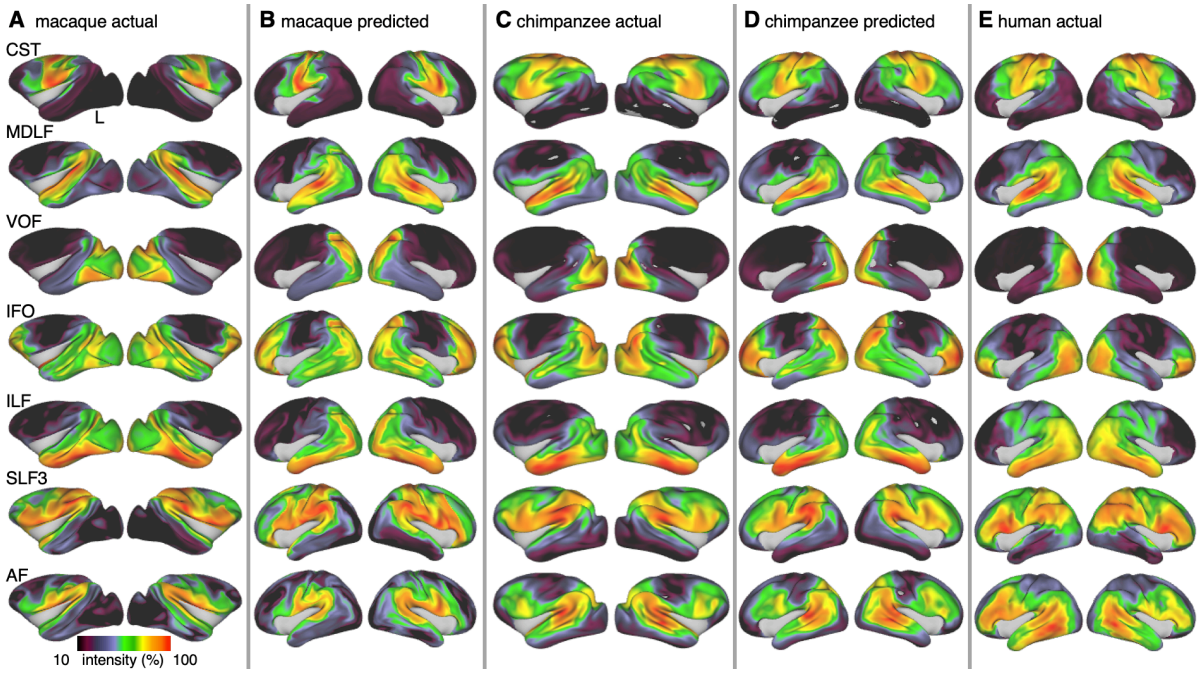

Figure 3. Actual and predicted tract maps. Actual tract maps of macaque (**A**), chimpanzee (**C**) and human (**E**). **B** and **D** show the tract maps in human space, predicted by the myelin-based registration for macaque and chimpanzee.

In the case of CST, the actual tract projections in the three species show terminations in pre- and post-central gyrus (Figure 3A). For the chimpanzee and macaque, these terminations span a relatively larger portion of the frontal cortex, while in the human the anterior part of the frontal lobe does not show any tract terminations. The frontal difference in the three actual tract maps is related to the relative increase in human prefrontal cortex, which is low in myelin content. After applying the myelin-based registration to the macaque and chimpanzee tract maps of CST, the predicted terminations in human space show strong overlap with the actual human tract map (Figure 4A). The myelin-based registration thus can model the effect of an increased prefrontal cortex on CST tract terminations. This overlap is captured in the weighted correlation maps, which have a high value in areas surrounding the central gyrus (Figure 4B,C). The Dice coefficients for the chimpanzee and macaque CST are relatively high (Figure 5A). The extension ratio is close to 1 in the left hemisphere and slightly elevated for the macaque right hemisphere.

The myelin-based registration also results in good prediction for tract projections in posterior temporal and parietal areas. The actual human tract terminations of MDLF, for example, span the superior temporal gyrus and reach the inferior parietal cortex (Figure 3E). In the macaque and chimpanzee, the actual MDLF terminates in superior temporal gyrus but reaches only a small part of the inferior parietal cortex. When applying the myelin-based registration, macaque and chimpanzee MDLF are both predicted to reach a comparable portion of the human temporal lobe and parts of both angular and supramarginal gyri of the inferior parietal lobe (Makris et al., 2013). The myelin-based registration thus predicts MDLF tract projections well resulting in a high Dice coefficient and a relatively low extension ratio.

A similar observation can be made for the posterior terminations of VOF and IFO. The myelin-based registration can predict the posterior cortical projections of those tracts to a large degree and the predicted cortical terminations of the tracts show a strong overlap with the actual human tract terminations. The termination zones of VOF are found in occipital lobe in all three species. Primary visual cortex has moved from the lateral surface in the macaque to the medial surface in the human, which is modelled well in our myelin registration. When applying the registration, macaque and chimpanzee VOF is predicted to reach posterior and medial parts of the occipital lobe, overlapping well with the actual human tract map. Dice coefficients for VOF are high in both species and the extension ratio close to 1. IFO is predicted to reach to anterior frontal and occipital areas. Due to the lower registration performance of the myelin maps in these areas (Figure S2), the anterior frontal terminations have to be interpreted with caution. In line with the overlay maps and the weighted correlation maps, the Dice coefficients are relatively high for these tracts. Taken together, this suggests that expansion and relocation of brain areas is largely sufficient to model the posterior cortical terminations of these tracts, while extension of the tracts' connectivity patterns plays a minor role in explaining the species differences.

The extension ratio for ILF and SLF3 are elevated indicating that there is some remaining tract extension that has not been modelled by cortical relocation. This is also reflected in the tract overlays (Fig. 4A), which shows that human ILF extends more into posterior temporoparietal cortex and SLF3 extends more into ventrolateral prefrontal cortex than is predicted by the myelin registration. Again, we note that frontal registration is less accurate and that these results should thus be interpreted with more caution. Thus, although the overall architecture

of the tracts is well predicted, these tracts seem to have extended a bit into new cortical territory in the human lineage.

The clearest case of a tract extension in the human brain was presented by AF. Human AF reaches anteriorly to inferior and dorsal frontal areas. The posterior projections of human AF reach into middle and inferior temporal cortex. AF in the chimpanzee shows weaker frontal terminations, reaching to inferior frontal, but to a lesser extent to dorsal frontal areas. The posterior terminations are in inferior parietal lobe and superior temporal cortex. In the macaque, the frontal terminations are notably reduced and the temporal projections reach superior temporal areas. For AF, the myelin-based registration does not provide a good prediction of the tract map across species, especially for the macaque. The correlation map for the chimpanzee shows a good prediction in frontal and parietal areas, but low correlation along the remaining temporal lobe. For the macaque, correlation values in both frontal and temporal lobe are extremely low. AF has the lowest Dice coefficient and the extension ratio is high, especially in the macaque, which is in line with overlay and correlation maps. This indicates that extension and relocation of cortical areas is not sufficient to explain the tract projections of AF, but that the tract extended into new cortical territory in the frontal and temporal lobe.

Connectivity fingerprints

To further characterize the effect of the reported features in the predicted tract maps, we obtained connectivity fingerprints at two representative vertices on the left brain surface: One in inferior parietal lobe, where most tracts are predicted well and one in the middle temporal gyrus, where we observed strong species differences in AF. Figure 5C demonstrates that for the inferior parietal lobe the connectivity fingerprint of actual human and predicted chimpanzee and macaque tract maps are highly similar, except for a small extension of the ILF as discussed above. This indicates that the myelin-derived registration can predict this area's connectivity profile well. For the temporal vertex, however, there is a strong mismatch regarding connectivity with the arcuate fasciculus, which indicates that the connectional fingerprint of this area is different in the human than would be predicted purely based on cortical relocation. Thus, the connectivity fingerprints of the two areas match the pattern that emerged from the results above.

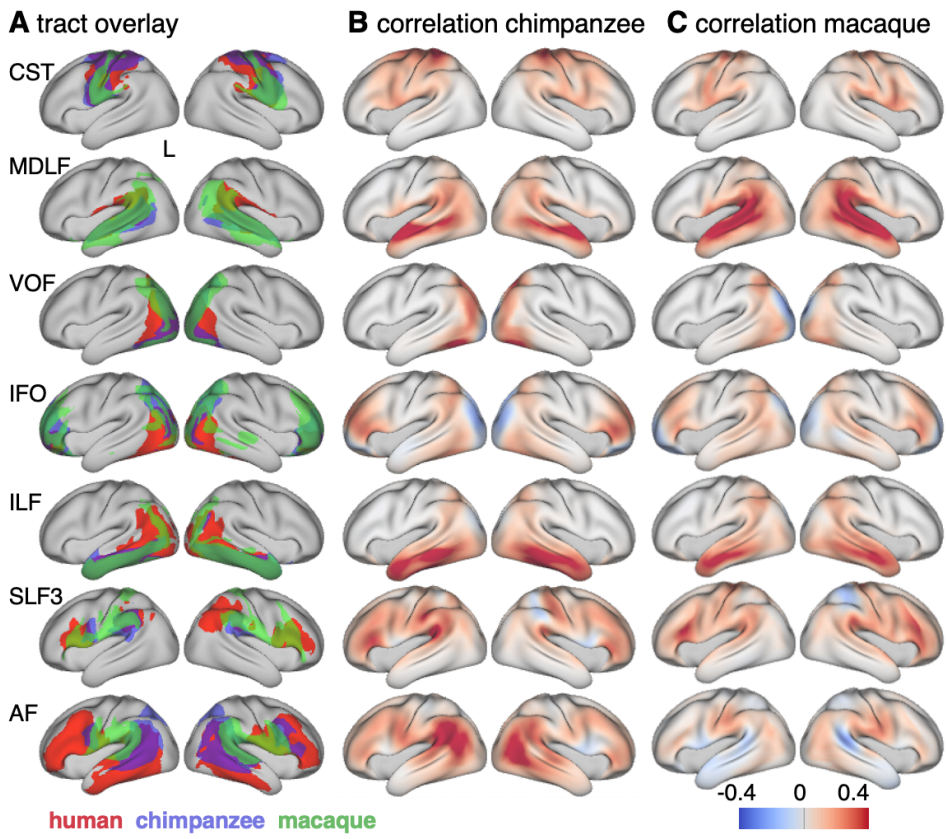

Figure 4. Cross-species comparison results. **A**: Thresholded actual human tract maps (red) and tract maps predicted by the myelin-based registration for chimpanzee (blue) and macaque (green) (thresholds (t): CST: t = 0.6, MDLF: t = 0.7, VOF: t = 0.6, IFO: t = 0.75, ILF: t = 0.7, SLF3: t = 0.85, AF: t = 0.75). **B**, **C**: Weighted correlation maps of actual human map and predicted chimpanzee and macaque map.

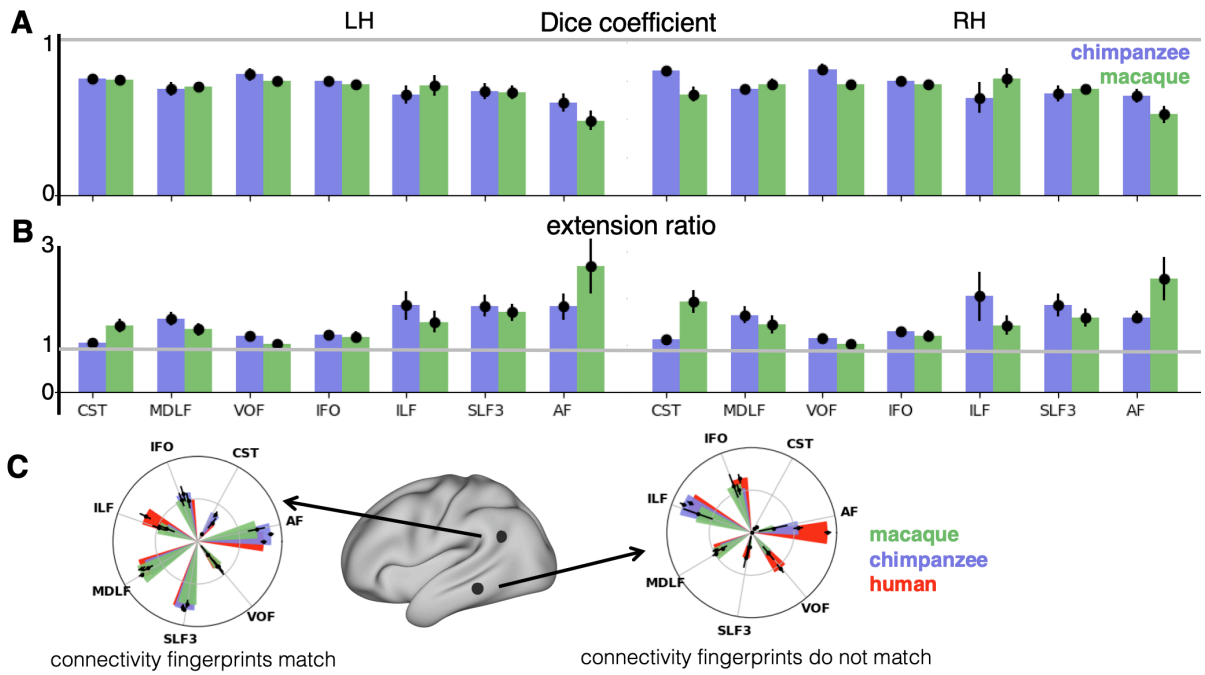

Figure 5. Quantification of cross-species comparison. Dice coefficients of overlap (**A**) and tract extension ratios (**B**) computed from thresholded human tract maps and tract maps predicted by the other species. Shown are mean and standard deviation derived from all pairs of human (n = 20) and macaque or chimpanzee (n = 5) subjects in left (LH) and right (RH) hemisphere. **C**: Connectional fingerprints at two vertices in parietal and temporal lobe. Shown are mean and standard deviation (human: n = 20, chimpanzee and macaque: n = 5).

Discussion

The goal of this study was to assess the differential effect of two forms of cortical reorganization to compare brain specializations across species: cortical relocation due to local expansions and extensions of tracts into new cortical territory (Figure 1). For this reason, we developed a cross-species surface registration method based on cortical myelin content, which gives us an index of how cortical areas have relocated during evolution. In a subsequent step, we tested if cortical relocation can predict the connectivity patterns of a set of tracts across species. We showed that cortical expansion and resulting relocation of brain areas alone provide a good prediction of several tracts' terminations in posterior temporal and parietal cortex. In the case of AF in particular, we showed that tract extension was an additional driving factor of brain reorganization.

We applied the myelin-based registration to the tract maps in macaque and chimpanzee to transform them into human space. In the case of CST, for example, the human tract projections can be predicted well by our cortical relocation model. This indicates that the pattern of cortical terminations changed according to the general expansion and relocation of brain areas, without additional extension into new regions of the brain. For tracts reaching to the temporo-parietal areas, such as MDLF, VOF, IFO, and to a lesser extend ILF and SLF3, the posterior tract projections can also be modelled well, despite the large distortions of target areas within the cortical sheet. These tracts seem to follow the evolutionary scenario

described in the upper row in Figure 1B,D, where a tract's extension in the human brain can be explained by relocation of areas along the cortical sheet.

AF showed the lowest consistency across species when applying the myelin-based registration. Dice ratio and extension ratio reflect the increased tract termination into frontal and temporal lobes, which can be observed in the tract maps. This points to further evolutionary adaptations that specifically affected the connectivity pattern of AF independent of cortical relocation, the scenario described in the bottom figure in Figure 1(B,D). Extending into new cortical territories changes the unique connectivity fingerprint of an area, which profoundly changes the computational capabilities that area supports (Figure 5C) (Rogier B Mars et al., 2018a). This result is consistent with previous accounts in the literature (Eichert et al., 2019b; Rilling et al., 2008), but the approach described here enabled us to formally test this hypothesis in the wider context of cortical reorganization across three primate species and to quantify the species differences.

The extension of AF into middle and inferior temporal cortical territory in the human brain is a hallmark of a number of models of human language processing (Hagoort, 2013; Roelofs, 2014), but more recently the role of ventral pathways is also highlighted (Catani and Bambini, 2014; Makris and Pandya, 2009; Saur et al., 2008). Here, we show that although both tracts have undergone relocation, AF in particular extends into new cortical territory and thus contributes to new, distinct connectivity fingerprints in the human brain. Our findings are in line with a recent comparative study of brain connectivity that found human-specific connections in inferior frontal gyrus and temporal lobe, when compared to the chimpanzee(Ardesch et al., 2019).

We noted some minor extensions of the SLF3 into ventrolateral prefrontal cortex and of ILF into temporoparietal cortex. Although we interpret the results of SLF3 with caution as the registration in frontal cortex is driven by fewer distinct myelin features than those in temporo-parietal cortex, there results are consistent with a previous study comparing human and chimpanzee SLF(Hecht et al., 2013). ILF's extension in the human brain is consistent with reports that in the human brain this tract has split into multiple subtracts (Latini et al., 2017; Roumazeilles et al., n.d.) due to the expansion of parts of the temporal cortex, including the fusiform gyrus. These extensions could be related to the increase of cortical territory related to processing social information, such as faces. These results thus provide an avenue for further experimental research into the function of these anatomical differences across species.

The tracts to test in our framework were chosen to have a good spread around the cortex, but our main focus was on temporo-parietal cortex. In fact, our myelin registration provides the best prediction of tract surface projections in the temporal, parietal and occipital cortex. Our approach allows us to explicitly transform data of multiple species into a common space, which makes evolutionary hypotheses directly testable, rather than 'eyeballing' the shared and distinct features. For instance, it has been previously suggested that the cortical projections of IFO are similar across primates (Mars et al., 2016), but our results provide more direct evidence for this hypothesis.

We adopted the MSM framework, which is ideally suited to work with multimodal descriptors of the cerebral cortex. It has become a vital tool for human surface registration (Abdollahi et al., 2014; Garcia et al., 2018; Glasser et al., 2016) and here we demonstrated its utility for cross-species research. With the presented surface matching method, we showed that a registration based on T1w/T2w MRI data can match critical landmarks across species. We have referred to these maps as 'myelin maps' in accordance with other studies in the literature (Glasser et al., 2014) but it should be noted that this is a heuristic. T1w/T2w maps are sensitive to other features than myelin and other sequences are sensitive to aspects of cortical myelin (Lutti et al., 2014). Importantly, the maps we employed here are similar across species, allowing us to compare like with like. As a result, the present approach can successfully model strong cortical expansion and resulting shifts using a region-of-interest-(ROI)-based initialization. We selected ROIs where the literature strongly suggests cross-species homology across primates (Glasser et al., 2014). Three ROIs were sufficient to bring the myelin maps into rough agreement in preparation for a second alignment step driven by whole brain myelin data.

The appearance of novel areas or topological variability, where regions swap around, cannot be modelled by the algorithm *per se*. However, smooth deformation algorithms have successfully been applied to study the emergence and maturation of cortical areas during brain development (Garcia et al., 2018) and cortical evolution(Lyu et al., 2015). MSM uses biomechanical regularization to minimize the impact of missing areas and we can model the expansion of the cortical sheet that is associated with the emergence of a novel brain areas.

A major benefit of the presented approach is that it can be flexibly modified to include a variety of cortical features, which can be compared across species. Myelin does not provide high contrast in the large human frontal cortex and, as such, it is difficult to provide a good registration in frontal areas. The effects we report can only be reliably interpreted within the spatial resolution of brain areas. More detailed and fine scale species differences and homology assignments are not possible with the data shown here. However, the current method can be generalized to any modality of cortical organization, so future studies can incorporate modalities that have greater contrast in this part of the brain such as neurite orientation dispersion and density imaging (NODDI) measures (Zhang et al., 2012) and resting state fMRI networks (Vincent et al., 2007).

In sum, here we present a framework for analyzing cortical reorganization between brains of different species, applying it in the first instance to cortical relocation of areas due to local expansion and white matter tract connectivity. This allowed us to formalize the changes that occurred in some of the major white matter tracts across different branches of the primate phylogenetic tree, illustrated by data from the Old-World macaque monkey, the chimpanzee great ape, and the human. Future work will expand this approach not only to different modalities, but also to a much wider range of species, which is now becoming increasing possible due to the availability of multi-species datasets (Heuer et al., 2018; Milham et al., 2018). This provides a crucial step towards the understanding of phylogenetic diversity across the primate brain.

Materials and Methods

Human Data and Pre-processing

Human data were acquired in 20 subjects (12 females, 18-40 years) on a 3T Siemens Prisma scanner with a 32-channel head coil. The study was approved by the Central University (of Oxford) Research Ethics Committee (CUREC, R55787/RE001) in accordance with the regulatory standards of the Code of Ethics of the World Medical Association (Declaration of Helsinki). All participants gave informed consent to their participation and were monetarily compensated for their participation.

High-resolution structural images were acquired using a (MPRAGE) T1w sequence (TR = 1900 ms; TE = 3.97 ms; flip angle = 8°; 192 mm FoV; voxel size 1 mm isotropic) and (SPC) T2w sequence (TR = 3200 ms; TE = 451 ms; 256 mm FoV; voxel size 1 mm isotropic; Grappa factor = 2). Diffusion-weighted (DW) MRI data were acquired in the same subjects using a sequence from the UK Biobank Project (Miller et al., 2016). In brief, we used a monopolar Stejskal-Tanner diffusion encoding scheme (Stejskal and Tanner, 1965). Sampling in *q*-space included 2 shells at b = 1000 and 2000 s/mm^2 (voxel size 2 mm, MB = 3). For each shell, 50 distinct diffusion-encoding directions were acquired (covering 100 distinct directions over the two *b*-values). Five b = 0 images were obtained together with additional three b = 0 images with the phase-encoding direction reversed.

T1w and T2w scans were pre-processed using the HCP-pipeline (Glasser et al., 2013) cloned from the 'OxfordStructural' - fork (https://github.com/lennartverhagen/Pipelines). The processing pipeline includes anatomical surface reconstruction using FreeSurfer and provides measures of sulcal depth and surface maps of cortical myelin content (Fischl, 2012; Jenkinson et al., 2012). The mean image of the T1w scans was divided by the mean image of the T2w scans to create a T1w/T2w image. The bias corrected T1w/T2w-ratio was mapped onto the mid-thickness surface using Connectome Workbench command-line tools. We refer to this surface map as T1w/T2w 'myelin map' (Glasser et al., 2014; Glasser and Van Essen, 2011). In order to create a human average myelin map, the subject's individual myelin maps were aligned using MSM. The myelin alignment was initialized using alignment based on maps of sulcal depth (parameters are provided in Table S1). To create the species average maps, we used an implementation of MSM that optimizes based on a first-order (pairwise) cost function to penalize against distortions, given that no excessive distortions were expected.

Human volume data were registered to the Montreal Neurological Institute standard space (MNI152) and surface data was transformed to a surface template space (fs_LR).

Chimpanzee Data and Pre-processing

In vivo chimpanzee structural MRI and DW-MRI data were obtained from the National Chimpanzee Brain Resource (www.chimpanzeebrain.org). Data were acquired at the Yerkes National Primate Research Center (YNPRC) at Emory University through separate studies covered by animal research protocols approved by YNPRC and the Emory University Institutional Animal Care and Use Committee (approval no. YER-2001206). These chimpanzee

MRI scans were obtained from a data archive of scans obtained prior to the 2015 implementation of U.S. Fish and Wildlife Service and National Institutes of Health regulations governing research with chimpanzees. All the scans reported in this publication were completed by the end of 2012.

T1w/T2w myelin maps were obtained from a group of 29 adult chimpanzees (all female), scanned at 0.8 mm isotropic resolution (Donahue et al., 2018; Glasser et al., 2014). DW-MRI data were obtained in a subset of five individuals. Acquisition and pre-processing was previously described (Li et al., 2013; Rogier B. Mars et al., 2018b). Two diffusion-weighted images (TR = 5900 ms; TE = 86 ms; 41 slices; 1.8 mm isotropic resolution) were acquired using a single-shot spin-echo echo planar sequence for each of 60 diffusion directions (b = 1000 s/mm^2), each with one of the possible left–right phase-encoding directions and 4 repeats, allowing for correction of susceptibility-related distortion. For each repeat of diffusion-weighted images, five images without diffusion weighting (b = 0 s/mm^2) were also acquired with matching imaging parameters.

Chimpanzee volume and surface data were registered to a standard space template based on 29 chimpanzee scans acquired at the YNPRC (Donahue et al., 2018). A species average myelin map was derived using MSM as described for the human.

Macaque Data and Pre-processing

Ex vivo DW-MRI data were obtained from four rhesus macaques (one female, age at death: range 4-14 years) using a 7T magnet. Data acquisition and DW-MRI pre-processing have been previously described in detail (Eichert et al., 2019b). Data were acquired using a 2D diffusion-weighted spin echo multi slice protocol with single line readout (DW-SEMS; TE = 25 ms; TR = 10 s; matrix size: 128 x 128; resolution 0.6 mm; number of slices: 128; slice thickness: 0.6 mm). Nine non-diffusion-weighted (b = 0 s/mm^2) and 131 diffusion-weighted (b = 4000 s/mm^2) volumes were acquired with diffusion encoding directions evenly distributed over the whole sphere, except in one monkey were 7 non-diffusion-weighted images and 128 diffusion directions were collected. This protocol and similar ones have previously shown to be sufficient for comparison with *in vivo* human data (see for example:(D'Arceuil et al., 2007; Dyrby et al., 2011; Eichert et al., 2019b; Mars et al., 2016)).

Additionally, *ex vivo* data from one male macaque were obtained (de Crespigny et al., 2005) and pre-processed as described previously (Jbabdi et al., 2013). Relevant imaging parameters for DW-MRI data were: 4.7T Oxford magnet equipped with BGA 12 gradients; 3D segmented spin-echo EPI 430 µm isotropic resolution, 8 shots, TE = 33 ms, TR = 350 ms, 120 isotropically distributed diffusion directions, b = 8000 s/mm^2. Despite the different scanning parameters, data quality was appropriate to allow pooling of the *ex vivo* data sets. *In vivo* data from the same macaque subjects was not available.

To obtain macaque T1w/T2w myelin maps, *in vivo* T1w and T2w scans data were obtained from a previous study on five separate rhesus macaques (4 females, age range 3.4 years - 11.75 years). Data acquisition and pre-processing of the macaque data have been described previously (Large et al., 2016). Procedures of the *in vivo* macaque data acquisition were

carried out in accordance with Home Office (UK) Regulations and European Union guidelines (EU directive 86/609/EEC; EU Directive 2010/63/EU).

Macaque surface reconstruction and average myelin maps were derived as described for the human. Macaque volume and surface data were registered to a standard space, which is based on data from 19 macaques acquired at YNPRC (Donahue et al., 2018, 2016).

Myelin-based Surface Registration

Our aim was to derive a cross-species registration to model expansion and relocation of cortical brain areas. Therefore, we performed registration based on average surface myelin maps in the three species using MSM with higher-order smoothness constraints (Ishikawa, 2014; Robinson et al., 2018). We derived a transformation of the cortical surface so that homologous myelin landmarks across species matched. The general processing steps were as follows, but a more detailed description of the methodology and an explanatory figure are provided in the Supplementary Material.

We obtained a 'chimpanzee-to-human' and a 'macaque-to-chimp' registration. A 'macaque-to-human' registration was derived as a concatenation of both registration stages to minimize the between-species distortions needed. As input for the registration we used the three species average myelin maps and we performed the registration for both hemispheres separately. We derived these registrations (macaque-to-chimpanzee and chimpanzee-to-human) because they allowed us to directly compare those brains that have the smallest phylogenetic distance. We are, of course, not implying that the three species evolved from one another.

In general, the registration was derived using two stages. The first stage was based on three regions-of-interest (ROIs) to handle the gross distortions that are involved in matching myelin landmarks across species. Two ROIs captured the highly myelinated precentral motor cortex (MC) and MT+ complex and a third ROI covered the medial wall (MW). We used MSM to obtain a registration so that the ROIs are roughly matched across species. In the second stage, the ROI-based registration was used as initialization for the subsequent alignment of the whole-hemisphere myelin maps. To derive a macaque-to-human registration, we resampled the average macaque myelin map to chimpanzee space using the MSM-derived macaque-to-chimpanzee registration. Then we aligned the resampled macaque map in chimpanzee space with that of the human while using the chimpanzee-to-human registration as initialization.

The quality of the registration performance was assessed by computing a local spatial correlation between the human myelin map and the result of the chimpanzee and macaque registration. Furthermore, we visualized the deformations underlying the registration in form of a surface distortion map. The methods and results for these two analyses are provided in the Supplementary Material.

Tractography

Human and chimpanzee DW-MRI data were pre-processed using tools from FDT (FMRIB's Diffusion Toolbox, part of FSL 5.0 (Smith et al., 2004)). We applied the TOPUP distortion correction tool followed by eddy-current distortion and motion correction (Andersson et al., 2003; Andersson and Sotiropoulos, 2016) as implemented in FSL. Macaque *ex vivo* DW-MRI data were processed using tools from FSL as implemented in an in-house MR Comparative Anatomy Toolbox (Mr Cat, www.neuroecologylab.org).

Pre-processed DW-MRI images were processed by fitting diffusion tensors (FSL's DTIFIT (Behrens et al., 2003)) and by fitting a model of local fiber orientations including crossing fibers (FSL's BedpostX (Behrens et al., 2007; Jbabdi et al., 2012)). Up to three fiber orientations per voxel were allowed. Tractography was performed using FSL's probtrackx2. Registration warp-fields between each subject's native space and standard space were created using FSL's FNIRT.

We performed tractography of the following tracts: Cortico-spinal tract (CST), middle longitudinal fasciculus (MDLF), vertical occipital fasciculus (VOF), inferior fronto-occipital fasciculus (IFO), inferior longitudinal fasciculus (ILF), the third branch of the superior longitudinal fasciculus (SLF3), and the arcuate fasciculus (AF). Placement of seed, waypoint, and exclusion masks was based on previous studies, in order to reconstruct known pathways for these tracts in all three species (human and macaque: (De Groot et al., 2013; Rogier B Mars et al., 2018b), protocols for AF: (Eichert et al., 2019b); chimpanzee: Bryant, Li, & Mars, in prep.). Masks were drawn in standard space and warped to native subject diffusion MRI space for probabilistic tractography. The resulting tractograms were normalized by dividing each voxel's value by the total number of streamlines that successfully traced the required route ('waytotal'). To decrease computational load for further processing all tractograms were down-sampled (human: 2 mm, chimpanzee: 1.5 mm, macaque: 1 mm).

Surface Tract Maps

To assess which part of the cortical grey matter might be reached by the tracts, we derived the surface representation of each individual tractogram using a matrix multiplication method described previously (Rogier B Mars et al., 2018b) (Figure S1B(2)).

We calculated whole-hemisphere vertex-wise connectivity matrices, tracking from the 20k-vertices mid-thickness surface to all voxels in the brain. These matrices were computed for both hemispheres and each subject individually in the three species. In the macaque we used the five subject's average mid-thickness in standard space as input for the computation instead of individual surfaces.

To rebalance the weights in the tracts to be more homogenous, connectivity values were weighted by the distance between vertex and voxel. A distance matrix across all vertices of the mid-thickness surface and all brain voxels was computed using MATLAB's pdist2-function resulting in a matrix of the same size as the connectivity matrix. Each element in the

connectivity matrix was then divided by the corresponding value in the vertex-to-voxel distance matrix. To decrease data storage load (approx. 10 GB per matrix) the weighted connectivity matrices of the five subjects were averaged for each hemisphere and species.

To visualize a tract's surface representation, we multiplied the averaged connectivity matrix with a tract's tractogram ('fdt_paths'). We refer to the tract surface representation here as 'tract map'. The approach described above decreases gyral bias in the resulting tract map notably when compared to surface-based tractography or surface projections of the tractogram. However, the method introduced spurious effects on the medial wall and insula cortex, which are generally not well captured in the tract map. Given that both areas are not of interest in this study, they were masked out for further analysis. Tract maps were derived for each subject and hemisphere separately. Individual surface maps were smoothed on the mid-thickness surface (human: 4 mm kernel (sigma for the gaussian kernel function), smoothing on individual surface; chimpanzee: 3 mm kernel, smoothing on average surface; macaque: 2 mm kernel, smoothing on average surface), logNorm-transformed and averaged across subjects.

Predicted Tract Maps

Next, we tested if our myelin-based registration can be used to predict the tract maps across the three species. We resampled individual chimpanzee and macaque tract maps to human space using the macaque-to-human and the chimpanzee-to-human registration (Figure S1B(3)). Intensity values in actual and predicted tract maps ranged from 0 to 1. We averaged all predicted tract maps and displayed the average map onto a human average surface (Q1-Q6_R440). For visual inspection we also assessed and show thresholded tract maps. Thresholds were chosen different for each tract, ranging from 0.6 to 0.85, so that the most characteristic termination is visible.

To visualize and quantify the prediction of macaque and chimpanzee tracts in human space, we derived weighted whole-hemisphere local correlation maps of the human map and the map predicted by macaque or chimpanzee. The local correlation map was computed using a sliding window around every vertex on the sphere using MATLAB's corrcoef-function (Mathworks, Natick, MA). We used a search kernel of 40° that corresponds to a circular search window with a radius of approximately 7 cm. The correlation map was modified to up-weight the brain areas where the tract is represented on the surface. A weighting mask was derived by multiplication of the intensities in the actual human tract map and the other species' predicted map. The values for the weighted correlation map are thus high in parts of the brain where both actual human and predicted tract show a termination, and where the spatial patterns of intensity values correlate. Weighted correlation maps were derived for each pair of 20 human subjects and five subjects of the other species. As result figure we display the averaged correlation map onto the human average surface.

In order to quantify how well a tract is predicted, we computed Dice coefficients of similarity (Dice, 1945), which quantifies the amount of overlap of the tract maps. The metric was derived for each pair of 20 human subjects and five subjects of the other species. The Dice coefficient was computed for the binarized and thresholded actual human tract map and the

map predicted by the other species. The threshold was chosen for each tract individually so that 40% of surface vertices were covered by the human tract map. As a quantification of tract extension, we computed the ratio of the number of vertices covered by the thresholded human tract map and the number of vertices covered by both the human and the other tract map. To confirm that the pattern of values is robust, both Dice coefficients and tract extension ratios were computed for a range of percentages of surface coverage and data for a coverage of 20%, 30% and 50% is provided in the Supplementary Material (Figure S3).

The differences in extension ratios at a surface coverage of 40% were assessed in a non-parametric permutation test implemented in PALM(Winkler et al., 2014) using 5000 permutations. A two-factorial model was fitted separately for both hemispheres to compare the main effects of species ('macaque' and 'chimpanzee') and tract and the interaction effect between the two factors. As the 100 data points for each tract and species were derived based on 20 human subjects and five subjects of the other species, we also modelled a random effect for each subject, i.e. we included 25 additional predictors. The *p*-values reported were corrected for family-wise error.

To demonstrate in which areas of the cortex connectivity can be explained well by cortical expansion, we computed connectivity fingerprints (Passingham et al., 2002) in two locations of the brain. Two vertices in the left human average surface were selected manually in the middle temporal gyrus and the inferior parietal lobe. Then we derived the value of all human tract maps and the tract maps predicted by the other species in each subject.

Acknowledgements

N.E. is a Wellcome Trust Doctoral student in Neuroscience at the University of Oxford [203730/Z/16/Z]. The project was supported by the NIHR Oxford Health Biomedical Research Centre. The Wellcome Centre for Integrative Neuroimaging is supported by core funding from the Wellcome Trust (203139/Z/16/Z). The work of R.B.M. is supported by the Biotechnology and Biological Sciences Research Council (BBSRC) UK [BB/N019814/1] and the Netherlands Organization for Scientific Research NWO [452-13-015]. The work of E.C.R. was supported by the Academy of Medical Sciences/the British Heart Foundation/the Government Department of Business, Energy and Industrial Strategy/the Wellcome Trust Springboard Award [SBF003\1116]. The work of K.L.B. is supported by a Marie Sklodowska-Curie Postdoctoral Research Fellowship from the European Commission [750026]. The work of S.J. is supported by the Medical Research Council UK [MR/L009013/1]. The work of M.J. is supported by the National Institute for Health Research (NIHR) Oxford Biomedical Research Centre (BRC). L.L.'s work is supported by the following grants: R01MH118534, P50MH100029, R01MH118285. Acquisition of the chimpanzee data was funded in part by the Yerkes National Primate Research Center Grant No. ORIP/OD P51OD011132; the Yerkes National Primate Center is supported by the National Institutes of Health, Office of Research Infrastructure Programs/OD [P51OD011132]; the National Chimpanzee Brain Resource is supported by NIH - National Institute of Neurological Disorders and Stroke. K.K.'s work is supported by the BBSRC UK [BB/H016902/1] and a Wellcome Trust Strategic Award [101092/Z/13/Z].

Author Contributions

Writing – Original draft: N.E., R.B.M.; Supervision and Project Administration: R.B.M.; Conceptualization: N.E., R.B.M.; Software: E.C.R.; Methodology: N.E., E.C.R., S.J., M.J., R.B.M.; Resources: N.E., K.L.B., L.L., K.K., R.B.M., K.E.W.; Writing – Review & Editing: N.E., E.C.R., K.L.B., S.J., M.J., K.K., K.E.W., R.B.M.; Funding Acquisition: N.E., R.B.M.

Declaration of Interests

The authors declare no competing interests.

Data Availability

All derived data supporting the findings of this study are available from the corresponding author upon request. Results scene files will be made available from the Wellcome Centre for Integrative Neuroimaging's GitLab at git.fmrib.ox.ac.uk/neichert/project_MSM.

Code Availability

Upon acceptance of the manuscript, code to run the between-species registration using MSM will be available from the Wellcome Centre for Integrative Neuroimaging's GitLab at git.fmrib.ox.ac.uk/neichert/project_MSM. FSL tools, including MSM, are available from fsl.fmrib.ox.ac.uk. Code for MSM using higher-order smoothness constrains is available online at https://www.doc.ic.ac.uk/~ecr05/MSM_HOCR_v2/. Connectome Workbench is available at www.humanconnectome.org/software/connectome-workbench.html.

Supplementary Material

Supplementary Methods

Myelin-based Surface Registration

We implemented a cross-species registration based on surface myelin maps using MSM (Figure S1A). MSM is a cortical surface registration algorithm, which works by projecting sheet-like models of the cortical surface to spheres; then aligning these by driving deformation of an input (or moving) mesh until features on the surface (i.e. myelin map intensities) increase in similarity with those represented on a fixed, or reference, mesh. We used a version of MSM that uses higher-order smoothness constraints and strain-based regularization for the regularization mode. MSM can work with multidimensional feature maps and use cross correlation across features to drive a registration. Multiple registration steps can be combined by using the output of a previous registration as initialization.

The main inputs of MSM were the average species myelin maps (Figure S1A(1)). All surface and metric files were resampled to a regular 20k-vertices mesh (radius of the sphere: 10 cm). For all species, the same sphere was used for re-sampling, so that the vertices had correspondence across species (Figure S1A(2)).

Given the substantial distortions that are required to match myelin landmarks across species, we initialized the myelin registration using a region-of-interest-(ROI)-driven registration. Three binary ROIs were manually drawn in Connectome Workbench's wb_view onto each species' myelin map (Figure S1A(3)). The value inside the ROI was 1 and outside 0. Two ROIs captured the highly myelinated precentral motor cortex (MC) and MT+ complex and a third ROI covered the medial wall (MW). The first initialization step aligned a single ROI for MT+ complex between species to facilitate alignment of the remaining two ROIs (Figure S1A(5)). Next, the three ROIs were combined in a multidimensional file, i.e. in a metric file that contained three data-arrays, or columns (Figure S1A(6)). MSM alignment of these sets of ROIs was initialized by the MT+ ROI registration (Figure S1A(9)). Initialization was performed using the '--trans=X.sphere.reg.surf.gii'-setting in the MSM-command. In the following step, the whole-hemisphere myelin maps were aligned by using the three-ROI registration step as initialization (Figure S1A(10)).

To derive a macaque-to-human registration, we resampled the macaque myelin map to chimpanzee space using the MSM-derived macaque-to-chimpanzee registration. Then we registered the resampled macaque map to the human map while using the chimpanzee-to-human registration as initialization. This approach allowed refinement of the macaque-to-human mapping rather than just applying the chimpanzee-to-human registration to the resampled map. The surface registration was derived for both hemispheres separately with mirrored versions of the ROIs. For registration steps involving ROIs, the registration sphere derived from the left hemisphere was flipped to the right hemisphere. For the steps using myelin maps, we derived the registration separately for the right hemisphere. Configuration parameters for all MSM-steps were determined empirically and were kept constant for the two hemispheres (all parameters are provided in Table S2).

The quality of the registration performance was visualized by computing a local spatial correlation between the human myelin map and the result of the chimpanzee and macaque registration. The correlation was computed using a sliding window around every vertex on the sphere using MATLAB's corrcoef-function (Mathworks, Natick, MA). We used a search kernel of 40° that corresponds to a circular search window with a radius of approximately 7 cm.

To visualize the shifts underlying the three cross-species registrations, we derived a map of surface distortions. We computed the areal distortion between original and distorted mesh, as implemented in 'wb_command -surface-distortion'. Here, distortions for each mesh face are estimated as $\log_2(A_1/A_0)$, where A_0 is the area of the original mesh face and A_1 is the area of a deformed mesh face. The values per vertex are calculated as a weighted average, where weights are calculated from the relative size of the vertices adjoining mesh faces. We are representing distortions between original and distorted sphere thus the numerical values of the distortion map are not meaningful.

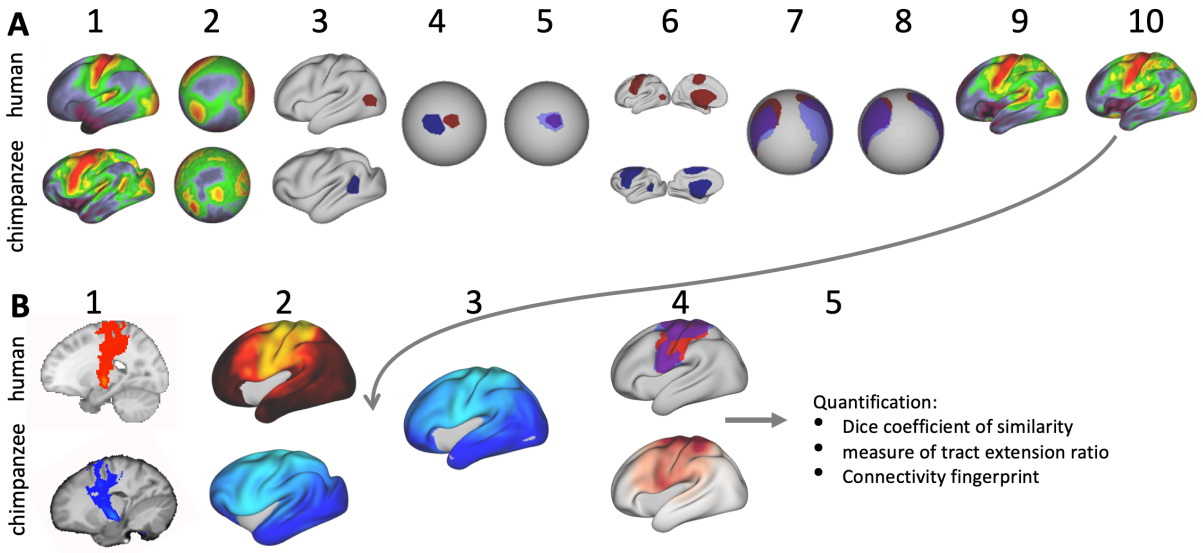

Figure S1. Related to Methods. **A**: MSM registration between chimpanzee and human myelin maps. (1) average species myelin maps. (2) myelin maps displayed on common sphere. (3) ROI for MT+ complex drawn on native surface. (4) MT+ ROI displayed on common sphere. (5) chimpanzee MT+ROI (blue) registered to human (red) using MSM. (6) Set of three ROIs (MC, MT+, MW). (7) Effect of MT+ ROI-derived initialization on the set of ROIs (only MW and MC visible). (8) Registration of chimpanzee set of ROIs to human ROIs using MSM. (9) Effect of ROI-derived registration on whole hemisphere chimpanzee myelin map. (10) Registration of whole brain myelin maps initialized by set of ROIs using MSM. **B**: Tract surface analysis. (1) Tractography result for example tract (CST). (2) Tract map obtained by matrix multiplication. (3): The myelin-derived cross-species registration (A10) is applied to transform the actual chimpanzee tract map to human space. (4) Having both tract maps in the same space allows a direct species comparison and quantification of the differences (5).

Supplementary Results

The performance of the myelin-based registration is visualized in the local correlation maps of actual human and predicted myelin maps (Figure S2A). The vast majority of the cortical myelin maps correlates well after applying the registration. The correlation map shows that inferior frontal parts of the cortex and anterior temporal lobe remain most dissimilar. Despite the good alignment of critical posterior landmarks, such as V1 and MT+ complex, the correlation in posterior parietal areas is lower than in more central areas indicating some residual dissimilarity in the registered myelin maps.

The deformations underlying the registration can be visualized using a surface distortion map, which is based on the logarithmic ratio of mesh triangle size before and after applying the transformation (Figure S2B). These expansions are underlying the shifts that lead to relocation of cortical areas. A value greater 1 indicates a relative increase of the underlying mesh triangles and a value below 1 indicates a relative decrease in size. Note that the overall increase in brain size across species is not accounted for in this calculation so that some areas show a distortion value smaller than 1. The macaque-to-chimpanzee distortion map demonstrates that the largest expansion happened in frontal areas. Other areas that show expansion are parietal cortex, posterior temporal and dorsal medial areas. The largest expansion from chimpanzee to human happened in superior temporal and prefrontal cortex, but the distortions are overall smaller and less extended than from macaque to chimpanzee. The macaque-to-human distortion map shows a similar pattern than chimpanzee-to-human, but indicates a stronger distortion in frontal areas.

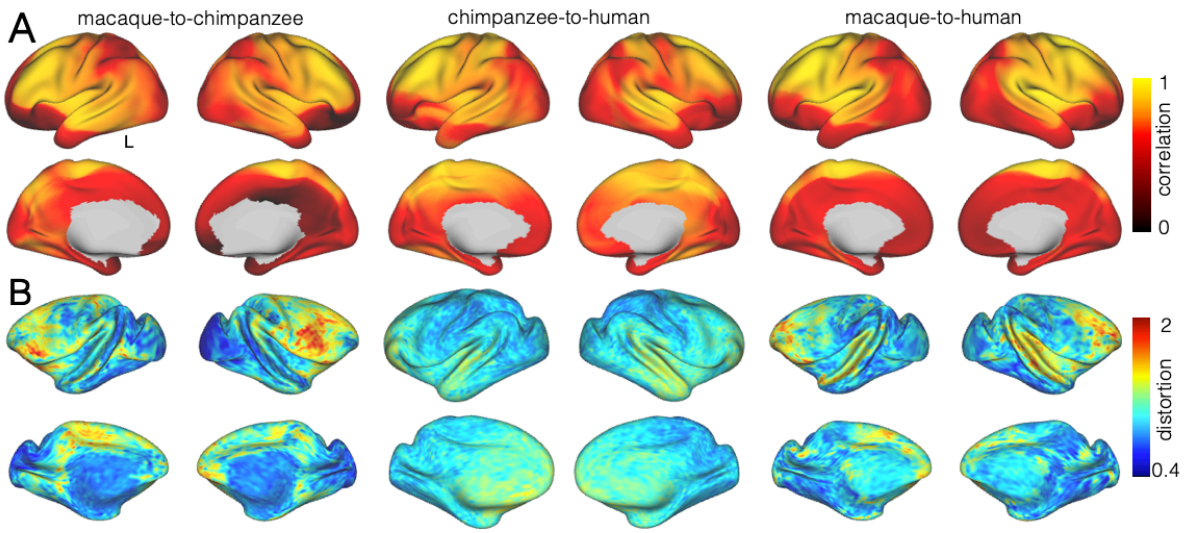

Figure S2. Related to Figure 2. Myelin correlation and mesh distortion. **A**: Local correlation of myelin maps after applying the MSM-derived registration. **B**: Relative distortion of the mesh underlying the registrations. The values indicate a relative expansion (>1) or contraction (<1) of the mesh.

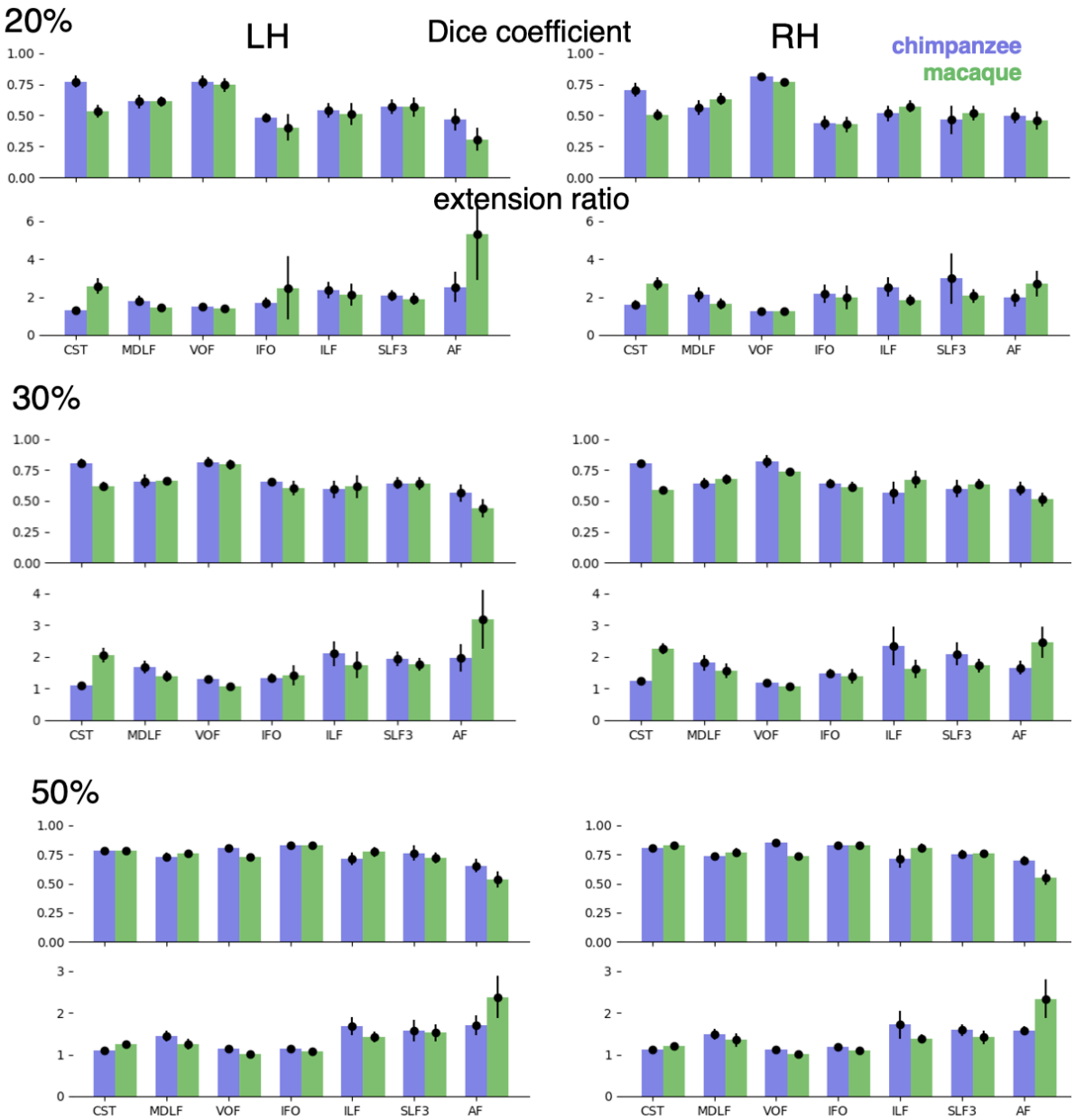

Figure S3. Related to Figure 5. Dice coefficients and tract extension ratios for different percentages of surface coverage. Shown are mean and standard deviation value derived from all pairs of human (*n* = 20) and macaque or chimpanzee (*n* = 5) subjects in left (LH) and right (RH) hemisphere.

<u>Supplementary Tables</u>

sulcal depth	myelin map
--simval=1,2,2,2 --sigma_in=4,4,2,1 --sigma_ref=2,2,1,1 --lambda=0,0.1,0.2,0.3 --it=50,3,3,3	--simval=2,2,2 --sigma_in=10,5,3 --sigma_ref=10,5,3 --lambda=0.1,0.1,0.3 --it=10,10,10

--opt=AFFINE,DISCRETE,DISCRETE,DISCRETE --CPgrid=0,2,3,4 --SGgrid=0,4,5,6 --datagrid=4,4,5,6 --IN levels=4	--opt=DISCRETE,DISCRETE,DISCRETE --CPgrid=2,3,4 --SGgrid=4,5,6 --datagrid=4,5,6 levels=3 (--trans: sulcal depth registration)

Table S1. Related to Methods. MSM configuration parameters for the registration of individual subject myelin maps prior to averaging to create a species myelin map. The parameters were kept constant for the three species and for both hemispheres.

macaque mesh as input	chimpanzee mesh as input
step: 4→5 macaque-to-chimpanzee: MT+ ROI --sigma_in=25 --lambda=0.1 --it=10 --opt=DISCRETE --CPgrid=1 --SGgrid=3 --regoption=3 --regexp=2 --dopt=HOCR --VN --triclique --k_exponent=2 --bulkmod=1 --shearmod=0.2 level=1	step: 4→5 chimpanzee-to-human: MT+ ROI --sigma_in=20,15,5 --lambda=0.05,0.1,0.1 --it=10,10,10 --opt=DISCRETE,DISCRETE,DISCRETE --CPgrid=2,3,4 --SGgrid=4,5,6 --regoption=3 --regexp=2 --dopt=HOCR --VN --triclique --k_exponent=2 --bulkmod=1 --shearmod=0.2 level=3
step: 7→8 macaque-to-chimpanzee: three ROIs --sigma_in=25,15,5 --lambda=0.01,0.01,0.1 --it=10,10,10 --opt=DISCRETE,DISCRETE,DISCRETE --CPgrid=1,2,3 --SGgrid=3,4,5 --regoption=3 --regexp=2 --dopt=HOCR --VN --triclique --k_exponent=2 --bulkmod=1 --shearmod=0.1	step: 7→8 chimpanzee-to-human: three ROIs --sigma_in=25 --lambda=0.001 --it=10 --opt=DISCRETE --CPgrid=2 --SGgrid=4 --regoption=3 --regexp=2 --dopt=HOCR --VN --triclique --k_exponent=2 --bulkmod=1 --shearmod=0.2

level=3 (--trans: single ROI registration)	level=1 (--trans: single ROI registration)
step: 9→10 macaque-to-chimpanzee: myelin map --sigma_in=10,5,3 --lambda=0.1,0.1,0.1 --it=10,10,20 --opt=DISCRETE,DISCRETE,DISCRETE --CPgrid=2,3,4 --SGgrid=4,5,6 --IN --excl --regoption=3 --regexp=2 --dopt=HOCR --triclique --k_exponent=2 --bulkmod=1 --shearmod=0.2 level=3 (--trans: three ROI registration)	step: 9→10 chimpanzee-to-human: myelin map --sigma_in=25,10,5 --lambda=0.2,0.5,0.5 --it=10,10,10 --opt=DISCRETE,DISCRETE,DISCRETE --CPgrid=2,3,4 --SGgrid=4,5,6 --regoption=3 --regexp=2 --dopt=HOCR --triclique --k_exponent=2 --bulkmod=1.6 --shearmod=0.1 level=3 (--trans: three ROI registration)
step: 9→10 macaque-to-human (input: macaque myelin map transformed by applying the macaque-to-chimpanzee registration) --sigma_in=25,10,5 --sigma_ref=25,10,5 --lambda=0.1,0.1,0.1 --it=10,10,3 --opt=DISCRETE,DISCRETE,DISCRETE --CPgrid=2,3,4 --SGgrid=4,5,6 --datagrid=4,5,6 --IN --regoption=3 --regexp=2 --dopt=HOCR --triclique --k_exponent=2 --bulkmod=1.6 --shearmod=0.1 level=3	

(--trans: chimpanzee-to-human myelin map registration)	

Table S2. Related to Methods 'Myelin-based Surface Registration'. MSM configuration parameters. Settings for the MSM command for registrations using the macaque data as input (left panel) and chimpanzee data as input (right panel). The described 'step' refers to the numbering in Figure S1A. Parameters were identical for the left and right hemisphere.

References

Abdollahi RO, Kolster H, Glasser MF, Robinson EC, Coalson TS, Dierker D, Jenkinson M, Van Essen DC, Orban GA. 2014. Correspondences between retinotopic areas and myelin maps in human visual cortex. *NeuroImage* **99**:509–524. doi:10.1016/j.neuroimage.2014.06.042

Andersson JLR, Skare S, Ashburner J. 2003. How to correct susceptibility distortions in spin-echo echo-planar images: Application to diffusion tensor imaging. *NeuroImage* **20**:870–888. doi:10.1016/S1053-8119(03)00336-7

Andersson JLR, Sotiropoulos SN. 2016. An integrated approach to correction for off-resonance effects and subject movement in diffusion MR imaging. *NeuroImage* **125**:1063–1078. doi:10.1016/j.neuroimage.2015.10.019

Ardesch DJ, Scholtens LH, Li L, Preuss TM, Rilling JK, van den Heuvel MP. 2019. Evolutionary expansion of connectivity between multimodal association areas in the human brain compared with chimpanzees. *Proceedings of the National Academy of Sciences* **116**:7101–7106. doi:10.1073/pnas.1818512116

Behrens TEJ, Johansen-Berg H, Jbabdi S, Rushworth MFS, Woolrich MW. 2007. Probabilistic diffusion tractography with multiple fibre orientations: What can we gain? *NeuroImage* **34**:144–155. doi:10.1016/j.neuroimage.2006.09.018

Behrens TEJ, Woolrich MW, Jenkinson M, Johansen-Berg H, Nunes RG, Clare S, Matthews PM, Brady JM, Smith SM. 2003. Characterization and Propagation of Uncertainty in Diffusion-Weighted MR Imaging. *Magnetic Resonance in Medicine* **50**:1077–1088. doi:10.1002/mrm.10609

Bryant K, Mars RB. 2019. Organization of extrastriate and temporal cortex in chimpanzees compared to humans and macaques (in press). *Cortex*.

Bryant KL, Li L, Mars RB. n.d. A white matter atlas of the chimpanzee brain and quantitative comparison with human and macaque (in prep).

Catani M, Bambini V. 2014. A model for Social Communication And Language Evolution and Development (SCALED). *Current Opinion in Neurobiology* **28**:165–171. doi:10.1016/j.conb.2014.07.018

D'Arceuil HE, Westmoreland S, de Crespigny AJ. 2007. An approach to high resolution diffusion tensor imaging in fixed primate brain. *NeuroImage* **35**:553–565. doi:10.1016/j.neuroimage.2006.12.028

de Crespigny AJ, D'Arceuil HE, Maynard KI, He J, McAuliffe D, Norbash A, Sehgal PK, Hamberg L, Hunter G, Budzik RF, Putman CM, Gonzalez RG. 2005. Acute studies of a new primate model of reversible middle cerebral artery occlusion. *Journal of stroke and cerebrovascular diseases : the official journal of National Stroke Association* **14**:80–7. doi:10.1016/j.jstrokecerebrovasdis.2004.12.005

De Groot M, Vernooij MW, Klein S, Ikram MA, Vos FM, Smith SM, Niessen WJ, Andersson JLR. 2013. Improving alignment in Tract-based spatial statistics: Evaluation and optimization of image registration. *NeuroImage* **76**:400–411. doi:10.1016/j.neuroimage.2013.03.015

Dice LR. 1945. Measures of the Amount of Ecologic Association Between Species. *Ecology* **26**:297–302. doi:10.2307/1932409

Donahue CJ, Glasser MF, Preuss TM, Rilling JK, Van Essen DC. 2018. Quantitative assessment of prefrontal cortex in humans relative to nonhuman primates. *Proceedings of the*

National Academy of Sciences **115**:E5183–E5192. doi:10.1073/pnas.1721653115
Donahue CJ, Sotiropoulos SN, Jbabdi S, Hernandez-Fernandez M, Behrens TE, Dyrby TB, Coalson T, Kennedy H, Knoblauch K, Van Essen DC, Glasser MF. 2016. Using Diffusion Tractography to Predict Cortical Connection Strength and Distance: A Quantitative Comparison with Tracers in the Monkey. *The Journal of Neuroscience* **36**:6758–6770. doi:10.1523/JNEUROSCI.0493-16.2016
Dyrby TB, Baaré WFC, Alexander DC, Jelsing J, Garde E, Søgaard L V. 2011. An ex vivo imaging pipeline for producing high-quality and high-resolution diffusion-weighted imaging datasets. *Human Brain Mapping* **32**:544–563. doi:10.1002/hbm.21043
Eichert N, Verhagen L, Folloni D, Jbabdi S, Khrapitchev AA, Sibson NR, Mantini D, Sallet J, Mars RB. 2019a. What is special about the human arcuate fasciculus? Lateralization, projections, and expansion. *Cortex* **118**:107–115. doi:10.1016/j.cortex.2018.05.005
Eichert N, Verhagen L, Folloni D, Jbabdi S, Khrapitchev AA, Sibson NR, Mantini D, Sallet J, Mars RB. 2019b. What is special about the human arcuate fasciculus? Lateralization, projections, and expansion. *Cortex* 1–9. doi:10.1016/j.cortex.2018.05.005
Fischl B. 2012. FreeSurfer. *NeuroImage*. doi:10.1016/j.neuroimage.2012.01.021
Garcia KE, Robinson EC, Alexopoulos D, Dierker DL, Glasser MF, Coalson TS, Ortinau CM, Rueckert D, Taber LA, Van Essen DC, Rogers CE, Smyser CD, Bayly P V. 2018. Dynamic patterns of cortical expansion during folding of the preterm human brain. *Proceedings of the National Academy of Sciences* **115**:3156–3161. doi:10.1073/pnas.1715451115
Glasser MF, Coalson TS, Robinson EC, Hacker CD, Harwell J, Yacoub E, Ugurbil K, Andersson J, Beckmann CF, Jenkinson M, Smith SM, Van Essen DC. 2016. A multi-modal parcellation of human cerebral cortex. *Nature* **536**:171–178. doi:10.1038/nature18933
Glasser MF, Goyal MS, Preuss TM, Raichle ME, Van Essen DC. 2014. Trends and properties of human cerebral cortex: Correlations with cortical myelin content. *NeuroImage*. doi:10.1016/j.neuroimage.2013.03.060
Glasser MF, Sotiropoulos SN, Wilson JA, Coalson TS, Fischl B, Andersson JL, Xu J, Jbabdi S, Webster M, Polimeni JR, Van Essen DC, Jenkinson M. 2013. The minimal preprocessing pipelines for the Human Connectome Project. *NeuroImage* **80**:105–124. doi:10.1016/j.neuroimage.2013.04.127
Glasser MF, Van Essen DC. 2011. Mapping Human Cortical Areas In Vivo Based on Myelin Content as Revealed by T1- and T2-Weighted MRI. *Journal of Neuroscience* **31**:11597–11616. doi:10.1523/JNEUROSCI.2180-11.2011
Hagoort P. 2013. MUC (memory, unification, control) and beyond. *Frontiers in Psychology* **4**:1–13. doi:10.3389/fpsyg.2013.00416
Hecht EE, Gutman DA, Bradley BA, Preuss TM, Stout D. 2015. Virtual dissection and comparative connectivity of the superior longitudinal fasciculus in chimpanzees and humans. *NeuroImage* **108**:124–137. doi:10.1016/j.neuroimage.2014.12.039
Hecht EE, Gutman DA, Preuss TM, Sanchez MM, Parr LA, Rilling JK. 2013. Process versus product in social learning: comparative diffusion tensor imaging of neural systems for action execution-observation matching in macaques, chimpanzees, and humans. *Cerebral cortex (New York, NY : 1991)* **23**:1014–24. doi:10.1093/cercor/bhs097
Heuer K, Gulban OF, Bazin P-L, Osoianu A, Valabregue R, Santin M, Herbin M, Toro R. 2018. Evolution of neocortical folding: A phylogenetic comparative analysis of MRI from 33 primate species. *bioRxiv* 379750. doi:10.1101/379750
Huk AC, Dougherty RF, Heeger DJ. 2002. Retinotopy and functional subdivision of human areas MT and MST. *The Journal of neuroscience : the official journal of the Society for*

Neuroscience **22**:7195–205. doi:20026661
Ishikawa H. 2014. Higher-order clique reduction without auxiliary variables. *Proceedings of the IEEE Computer Society Conference on Computer Vision and Pattern Recognition* 1362–1369. doi:10.1109/CVPR.2014.177
Jbabdi S, Lehman JF, Haber SN, Behrens TE. 2013. Human and Monkey Ventral Prefrontal Fibers Use the Same Organizational Principles to Reach Their Targets: Tracing versus Tractography. *The Journal of neuroscience : the official journal of the Society for Neuroscience* **33**:3190–3201. doi:10.1523/JNEUROSCI.2457-12.2013
Jbabdi S, Sotiropoulos SN, Savio AM, Graña M, Behrens TEJ. 2012. Model-based analysis of multishell diffusion MR data for tractography: How to get over fitting problems. *Magnetic Resonance in Medicine* **68**:1846–1855. doi:10.1002/mrm.24204
Jenkinson M, Beckmann CF, Behrens TEJ, Woolrich MW, Smith SM. 2012. FSL. *NeuroImage* **62**:782–790. doi:10.1016/j.neuroimage.2011.09.015
Krubitzer L. 2009. In search of a unifying theory of complex brain evolution. *Annals of the New York Academy of Sciences* **1156**:44–67. doi:10.1111/j.1749-6632.2009.04421.x
Krubitzer L, Kaas J. 2005. The evolution of the neocortex in mammals: How is phenotypic diversity generated? *Current Opinion in Neurobiology*. doi:10.1016/j.conb.2005.07.003
Large I, Bridge H, Ahmed B, Clare S, Kolasinski J, Lam WW, Miller KL, Dyrby TB, Parker AJ, Smith JET, Daubney G, Sallet J, Bell AH, Krug K. 2016. Individual Differences in the Alignment of Structural and Functional Markers of the V5/MT Complex in Primates. *Cerebral Cortex* **26**:3928–3944. doi:10.1093/cercor/bhw180
Latini F, Mårtensson J, Larsson EM, Fredrikson M, Åhs F, Hjortberg M, Aldskogius H, Ryttlefors M. 2017. Segmentation of the inferior longitudinal fasciculus in the human brain: A white matter dissection and diffusion tensor tractography study. *Brain Research* **1675**:102–115. doi:10.1016/j.brainres.2017.09.005
Li L, Hu X, Preuss TM, Glasser MF, Damen FW, Qiu Y, Rilling J. 2013. Mapping putative hubs in human, chimpanzee and rhesus macaque connectomes via diffusion tractography. *NeuroImage* **80**:462–474. doi:10.1016/j.neuroimage.2013.04.024
Lutti A, Dick F, Sereno MI, Weiskopf N. 2014. Using high-resolution quantitative mapping of R1 as an index of cortical myelination. *NeuroImage* **93**:176–188. doi:10.1016/j.neuroimage.2013.06.005
Lyu I, Kim SH, Seong JK, Yoo SW, Evans A, Shi Y, Sanchez M, Niethammer M, Styner MA. 2015. Robust estimation of group-wise cortical correspondence with an application to macaque and human neuroimaging studies. *Frontiers in Neuroscience* **9**:210. doi:10.3389/fnins.2015.00210
Makris N, Pandya DN. 2009. The extreme capsule in humans and rethinking of the language circuitry. *Brain Structure and Function* **213**:343–358. doi:10.1007/s00429-008-0199-8
Makris N, Preti MG, Wassermann D, Rathi Y, Papadimitriou GM, Yergatian C, Dickerson BC, Shenton ME, Kubicki M. 2013. Human middle longitudinal fascicle: Segregation and behavioral-clinical implications of two distinct fiber connections linking temporal pole and superior temporal gyrus with the angular gyrus or superior parietal lobule using multi-tensor tractography. *Brain Imaging and Behavior* **7**:335–352. doi:10.1007/s11682-013-9235-2
Mars Rogier B., Eichert N, Jbabdi S, Verhagen L, Rushworth MFS. 2018a. Connectivity and the search for specializations in the language-capable brain. *Current Opinion in Behavioral Sciences* **21**:19–26. doi:10.1016/j.cobeha.2017.11.001
Mars RB, Foxley S, Verhagen L, Jbabdi S, Sallet J, Noonan MAP, Neubert FX, Andersson JL,

Croxson PL, Dunbar RIM, Khrapitchev AA, Sibson NR, Miller KL, Rushworth MFS. 2016. The extreme capsule fiber complex in humans and macaque monkeys: a comparative diffusion MRI tractography study. *Brain Structure and Function* **221**:4059–4071. doi:10.1007/s00429-015-1146-0

Mars Rogier B., O'Muircheartaigh J, Folloni D, Li L, Glasser MF, Jbabdi S, Bryant KL. 2018b. Concurrent analysis of white matter bundles and grey matter networks in the chimpanzee. *Brain Structure and Function* **0**:0. doi:10.1007/s00429-018-1817-8

Mars Rogier B, Passingham RE, Jbabdi S. 2018a. Connectivity Fingerprints: From Areal Descriptions to Abstract Spaces. *Trends in Cognitive Sciences*. doi:10.1016/j.tics.2018.08.009

Mars RB, Passingham RE, Neubert FX, Verhagen L, Sallet J. 2017. Evolutionary specializations of the human association cortex In: Kaas HJ, editor. Evolution of Nervous Systems. Oxford: Elsevier. pp. 1–37. doi:10.1016/B978-0-12-804042-3.00118-4

Mars RB, Sallet J, Neubert FX, Rushworth MFS. 2013. Connectivity profiles reveal the relationship between brain areas for social cognition in human and monkey temporoparietal cortex. *Proceedings of the National Academy of Sciences* **110**:10806–10811. doi:10.1073/pnas.1302956110

Mars Rogier B, Sotiropoulos SN, Passingham RE, Sallet J, Verhagen L, Khrapitchev AA, Sibson N, Jbabdi S. 2018b. Whole brain comparative anatomy using connectivity blueprints. *eLife* **7**. doi:10.7554/elife.35237

Milham MP, Ai L, Koo B, Xu T, Amiez C, Balezeau F, Baxter MG, Blezer ELA, Brochier T, Chen A, Croxson PL, Damatac CG, Dehaene S, Everling S, Fair DA, Fleysher L, Freiwald W, Froudist-Walsh S, Griffiths TD, Guedj C, Hadj-Bouziane F, Ben Hamed S, Harel N, Hiba B, Jarraya B, Jung B, Kastner S, Klink PC, Kwok SC, Laland KN, Leopold DA, Lindenfors P, Mars RB, Menon RS, Messinger A, Meunier M, Mok K, Morrison JH, Nacef J, Nagy J, Rios MO, Petkov CI, Pinsk M, Poirier C, Procyk E, Rajimehr R, Reader SM, Roelfsema PR, Rudko DA, Rushworth MFS, Russ BE, Sallet J, Schmid MC, Schwiedrzik CM, Seidlitz J, Sein J, Shmuel A, Sullivan EL, Ungerleider L, Thiele A, Todorov OS, Tsao D, Wang Z, Wilson CRE, Yacoub E, Ye FQ, Zarco W, Zhou Y di, Margulies DS, Schroeder CE. 2018. An Open Resource for Non-human Primate Imaging. *Neuron* **100**:61-74.e2. doi:10.1016/j.neuron.2018.08.039

Miller KL, Alfaro-Almagro F, Bangerter NK, Thomas DL, Yacoub E, Xu J, Bartsch AJ, Jbabdi S, Sotiropoulos SN, Andersson JLR, Griffanti L, Douaud G, Okell TW, Weale P, Dragonu I, Garratt S, Hudson S, Collins R, Jenkinson M, Matthews PM, Smith SM. 2016. Multimodal population brain imaging in the UK Biobank prospective epidemiological study. *Nature Neuroscience* **19**:1523–1536. doi:10.1038/nn.4393

Passingham RE, Stephan KE, Kotter R. 2002. The anatomical basis of functional localization in the cortex. *Nat Rev Neurosci* **3**:606–16. doi:10.1038/nrn893

Rilling JK, Glasser MF, Preuss TM, Ma X, Zhao T, Hu X, Behrens TEJ. 2008. The evolution of the arcuate fasciculus revealed with comparative DTI. *Nature Neuroscience* **11**:426–428. doi:10.1038/nn2072

Robinson EC, Garcia K, Glasser MF, Chen Z, Coalson TS, Makropoulos A, Bozek J, Wright R, Schuh A, Webster M, Hutter J, Price A, Cordero Grande L, Hughes E, Tusor N, Bayly P V, Van Essen DC, Smith SM, Edwards AD, Hajnal J, Jenkinson M, Glocker B, Rueckert D. 2018. Multimodal surface matching with higher-order smoothness constraints. *NeuroImage* **167**:453–465. doi:10.1016/j.neuroimage.2017.10.037

Robinson EC, Jbabdi S, Andersson J, Smith S, Glasser MF, Van Essen DC, Burgess G, Harms

MP, Barch DM, Jenkinson M. 2013. Multimodal surface matching: Fast and generalisable cortical registration using discrete optimisationLecture Notes in Computer Science (Including Subseries Lecture Notes in Artificial Intelligence and Lecture Notes in Bioinformatics). pp. 475–486. doi:10.1007/978-3-642-38868-2_40

Robinson EC, Jbabdi S, Glasser MF, Andersson J, Burgess GC, Harms MP, Smith SM, Van Essen DC, Jenkinson M. 2014. MSM: A new flexible framework for multimodal surface matching. *NeuroImage* **100**:414–426. doi:10.1016/j.neuroimage.2014.05.069

Roelofs A. 2014. A dorsal-pathway account of aphasic language production: The WEAVER++/ARC model. *Cortex* **59**:33–48. doi:10.1016/j.cortex.2014.07.001

Roumazeilles L, Bryant KL, Eichert N, Folloni D, Vijayakumar S, Reveley C, Verhagen L, Jbabdi S, Foxley S, Miller KL, Mars RB. n.d. Longitudinal connections of the temporal cortex in monkeys, great apes, and humans. *manuscript submitted for publication*.

Ruschel M, Knösche TR, Friederici AD, Turner R, Geyer S, Anwander A. 2014. Connectivity architecture and subdivision of the human inferior parietal cortex revealed by diffusion MRI. *Cerebral Cortex* **24**:2436–2448. doi:10.1093/cercor/bht098

Saur D, Kreher BW, Schnell S, Kümmerer D, Kellmeyer P, Vry M-S, Umarova R, Musso M, Glauche V, Abel S, Huber W, Rijntjes M, Hennig J, Weiller C. 2008. Ventral and dorsal pathways for language. *Proceedings of the National Academy of Sciences of the United States of America* **105**:18035–40. doi:10.1073/pnas.0805234105

Smith SM, Jenkinson M, Woolrich MW, Beckmann CF, Behrens TEJ, Johansen-Berg H, Bannister PR, De Luca M, Drobnjak I, Flitney DE, Niazy RK, Saunders J, Vickers J, Zhang Y, De Stefano N, Brady JM, Matthews PM. 2004. Advances in functional and structural MR image analysis and implementation as FSLNeuroImage. pp. S208–S219. doi:10.1016/j.neuroimage.2004.07.051

Stejskal EO, Tanner JE. 1965. Spin diffusion measurements: spin echoes in the presence of a time-dependant field gradient. *The Journal of chemical physics* **42**:288–292. doi:10.1063/1.1695690

Striedter GF, Belgard TG, Chen CC, Davis FP, Finlay BL, Güntürkün O, Hale ME, Harris JA, Hecht EE, Hof PR, Hofmann HA, Holland LZ, Iwaniuk AN, Jarvis ED, Karten HJ, Katz PS, Kristan WB, Macagno ER, Mitra PP, Moroz LL, Preuss TM, Ragsdale CW, Sherwood CC, Stevens CF, Stüttgen MC, Tsumoto T, Wilczynski W. 2014. NSF workshop report: Discovering general principles of nervous system organization by comparing brain maps across species. *Journal of Comparative Neurology* **522**:1445–1453. doi:10.1002/cne.23568

Thiebaut de Schotten M, Croxson PL, Mars RB. 2019. Large-scale comparative neuroimaging: Where are we and what do we need? *Cortex*. doi:10.1016/j.cortex.2018.11.028

Van Essen DC, Dierker DL. 2007. Surface-Based and Probabilistic Atlases of Primate Cerebral Cortex. *Neuron* **56**:209–225. doi:10.1016/j.neuron.2007.10.015

Vincent JL, Patel GH, Fox MD, Snyder LH, Baker JT, Van Essen DC, Zempel JM, Snyder AZ, Corbetta M, Raichle ME. 2007. Intrinsic functional architecture in the anaesthetized monkey brain. *Nature* **447**:83–86. doi:10.1038/nature05758

Winkler AM, Ridgway GR, Webster MA, Smith SM, Nichols TE. 2014. Permutation inference for the general linear model. *NeuroImage* **92**:381–397. doi:10.1016/j.neuroimage.2014.01.060

Zhang H, Schneider T, Wheeler-Kingshott CA, Alexander DC. 2012. NODDI: Practical in vivo neurite orientation dispersion and density imaging of the human brain. *NeuroImage* **61**:1000–1016. doi:10.1016/j.neuroimage.2012.03.072

1087